Simulation of Pellet-Cladding interaction with the PLEIADES fuel performance software environment

B. Michel, C. Nonon, J. Sercombe, F. Michel, V. Marelle

SIMULATION OF PELLET-CLADDING INTERACTION WITH THE PLEIADES FUEL PERFORMANCE SOFTWARE ENVIRONMENT

B. MICHEL, C. NONON, J. SERCOMBE, F. MICHEL, and V. MARELLE*
DEC0SESC bat 151 CEA de Cadarache 13108 Saint Paul Lez Durance France

This paper focuses on the PLEIADES fuel performance software environment and its application to the modeling of pellet-cladding interaction (PCI). The PLEIADES platform has been under development for 10 yr; a unified software environment, including the multidimensional finite element solver CAST3M, has been used to develop eight computation schemes now under operation. Among the latter, the ALCYONE application is devoted to pressurized water reactor fuel rod behavior. This application provides a three-dimensional (3-D) model for a detailed analysis of fuel element behavior and enables validation through comparing simulation and postirradiation examination results (cladding residual diameter and ridges, dishing filling, pellet cracking, etc.). These last years the 3-D computation scheme of the ALCYONE application has been enriched with a complete set of physical models to take into account thermomechanical and chemical-physical behavior of the fuel element under irradiation. These models have been validated through the ALCYONE application on a large experimental database composed of approximately 400 study cases. The strong point of the ALCYONE application concerns the local approach of stress-corrosion-cracking rupture under PCI, which can be computed with the 3-D finite element solver.

Further developments for PCI modeling in the PLEIADES platform are devoted to a new mesh refinement method for assessing stress-and-strain concentration (multigrid technique) and a new component for assessing fission product chemical recombination.

I. INTRODUCTION

Pellet-cladding-interaction (PCI) failures, discovered in the early 1970s, can be avoided in electro-nuclear reactors thanks to optimized plant operational procedures and fuel management schemes. Research and development (R&D) programs are however still undertaken worldwide on this subject in order to improve the understanding of the mechanisms possibly leading to PCI failure, as well as to qualify a PCI-resistant rod design. These R&D programs associate experimental and modeling approaches in order to better assess each elementary mechanism and to optimize the objectives and the number of experiments. As a result of the PCI-modeling needs, numerical simulation has been widely developed in order to provide a more detailed multidimensional assessment including nonlinear behavior under irradiation. The aim of this paper is to present the PLEIADES numerical environment developed in the last 10 yr in France in the framework of an experimental and research cooperative program between Electricité de France (EdF), AREVA, and the Commissariat à l'Énergie Atomique et aux Énergies Alternatives (CEA). First-generation CEA fuel performance codes have been fully implemented in the PLEIADES platform applications. The EdF fuel performance code CYRANO3 has been available in the PLEIADES platform since 2004 thanks to the codevelopment project. Now, the PLEIADES platform applications are the reference for fuel R&D at CEA and in the framework of the EdF-CEA-AREVA partnership.

In Secs. II and III, the PLEIADES multiconcept fuel software environment and fuel simulation algorithms are presented. In Sec. IV, numerical simulation results obtained for the pressurized water reactor (PWR) fuel rod

*E-mail: bruno.michel@cea.fr

concept are detailed. In Sec. V, computation of strain-and-stress concentration for stress-corrosion-cracking (SCC) failure assessment is discussed through three-dimensional (3-D) simulation results and new numerical development underway.

II. THE PLEIADES FUEL SOFTWARE ENVIRONMENT

The purpose of the PLEIADES project[1] has been to create a new simulation platform to study the behavior of nuclear fuels. The three main parts of the PLEIADES environment are described in Fig. 1. The architecture provides generic tools for multiphysics algorithms, data exchange [based on the SALOME software (http://www.salome-platform.org)], and linking with fuel databases. It also provides SALOME tools for preprocessing and postprocessing with user-friendly interfaces. The second part of the PLEIADES platform is a physical component library for fuel simulation embedded in C++ classes in a unified software environment. The third part consists of a generic computation algorithm, built with the architecture and the physical component library, with a user interface dedicated to each fuel concept. At the present time there are eight computation schemes under operation in the PLEIADES platform (see Fig. 2). Six of them are dedicated to specific fuel concept studies and provide a large validation database shared among CEA, EDF, and AREVA. The V.E.R computation scheme is devoted to simulation at the volume element scale for generic fuel microstructure analyses. The LICOS computation scheme is used for preliminary fuel design studies on nonstandard geometry. PCI modeling studies are achieved with the ALCYONE computation scheme, which provides a multidimensional approach for the PWR fuel rod concept.

III. FUEL SIMULATION ALGORITHM

IIIA. Multiphysics Problem

The main phenomena involved in fuel behavior modeling under irradiation are presented in Fig. 1. These phenomena can be separated into two problems: a neutronic and thermohydraulic problem and a nonlinear multiphysics problem for fuel element behavior under irradiation. The first problem is devoted to computing the nuclear power deposition in the fuel and power evacuation from the fuel element toward the energy conversion system. The second problem is devoted to computing the temperature distribution in the fuel element, mechanical fields, and structural material changes due to irradiation effects. Neutronic and thermohydraulic problems

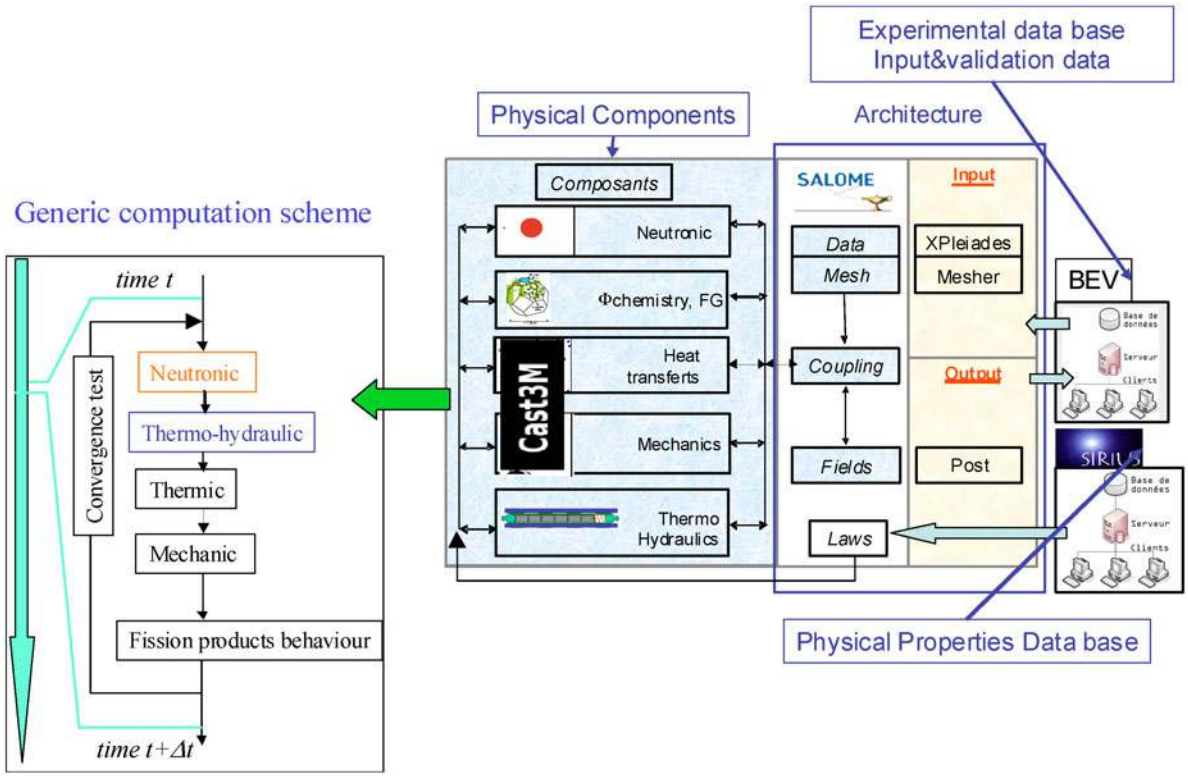

Fig. 1. PLEIADES software environment.

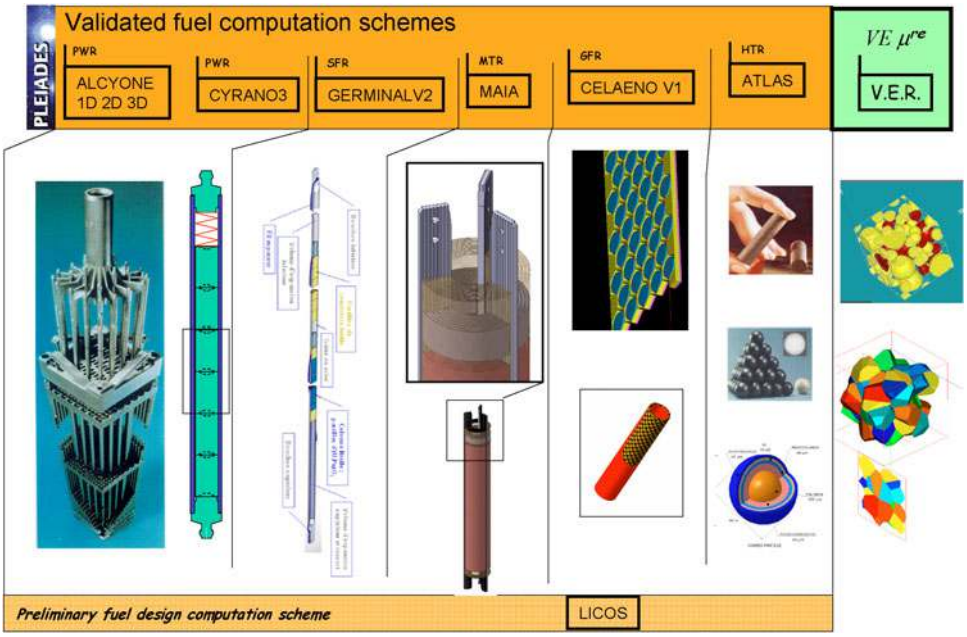

Fig. 2. PLEIADES computation schemes under operation.

are strongly linked to computations at the scale of the fuel assembly or reactor core. Thermal and mechanical computations are more relevant to the fuel element scale commonly used for assessing structural integrity, when a physicochemical computation is mainly linked to mechanisms at an atomistic scale (densification and solid swelling processes and gaseous fission product behavior).

IIIB. Nuclear Power Deposition Computation

The power density distribution through the pellet is computed with a simplified approach coming from the METEOR first-generation fuel performance code.[2] This approach is based on the one-dimensional (1-D) axisymmetric assumption first proposed by Palmer et al. in the RADAR model[3] where the solution of the coupling Boltzmann and Bateman constitutive equations is given by Eq. (1):

$$P_V^{local} \infty \Phi(r) \cdot \sum_{pf} \bar{\sigma}_{pf} \cdot C_{pf}(r) \cdot E_{pf} \quad , \tag{1}$$

where

$\Phi(r)$ = neutron flux

$\bar{\sigma}_{pf}$ = mean value of the one-group fission cross section of each fissile atom (subscript pf)

$C_{pf}(r) \cdot E_{pf}$ = concentration of each fissile atom multiplied by its corresponding fission energy.

The shape factor of the neutron flux $\Phi(r)$ is derived from the simple one-group diffusion theory,[4] and the mean value is fitted in order to have a total power per unit length of fuel equal to the prescribed value. The mean value of the one-group fission cross section is fitted, as a function of the burnup, with the results of the Boltzmann transport equation computation at the core scale. The fissile atom concentration is derived from the PRODHEL model,[5] which also computes the nonfissile atom concentration and will replace in the PLEIADES platform the extended version of the RADAR model previously used in METEOR.

IIIC. Thermohydraulic Computation

The thermohydraulic computation is devoted to assess the temperature of the heat transfer fluid and the wall heat transfer coefficient of the fuel element cladding. This temperature is then used as a boundary condition of the thermal problem in the fuel element (see Sec. III.D). Under nominal and transient irradiation conditions, the thermohydraulic model used for a light water reactor's fuel rod takes into account homogeneous two-phase flow in either the permanent or the transient stages. This model requires a boundary condition coming from the measured temperature at the bottom of the fuel rod.

IIID. Thermal Computation

The temperature distribution through the fuel element is computed according to the principle given by Eq. (2):

$$\rho \cdot c_p \cdot \frac{dT}{dt} + \text{div}\, \lambda\, \text{grad}\, T + p_V^{local} = 0 \ . \tag{2}$$

Heat transfer to the fluid is taken into account with the flux boundary condition given by Eq. (3):

$$\Phi = h \cdot (T_{wall} - T_\infty) \ , \tag{3}$$

where

h = wall heat transfer coefficient

T_∞ = heat transfer fluid temperature computed in the thermohydraulic model

λ = thermal conductivity of the irradiated material.

Concerning the heat flux through the pellet-cladding interface, we use an equivalent convection exchange coefficient to take into account conduction and radiation when a gap is opened or thermal resistance when a gap is closed.

IIIE. Mechanical Computation

The mechanical state of the fuel element is computed with the static equilibrium Eq. (4) integrated according to a weak formulation with the finite element method:

$$\text{div}\, \bar{\bar{\sigma}} = 0 \ . \tag{4}$$

In addition to this equilibrium principle, the nonlinear behavior of the fuel element is taken into account through several mechanical models with constitutive equations for the pellet, cladding, and pellet-cladding interface, as discussed below.

III.E.1. Pellet

Uncompressible viscoplastic behavior under irradiation is taken into account in the pellet [Eq. (5)]:

$$\frac{d\varepsilon_{creep}}{dt} = \text{Max}[A_i(p, D_G) \cdot (J_2(\bar{\bar{\sigma}}))^{n_i} \cdot e^{-Q_i/R \cdot T}] \cdot \left(1 + \alpha \cdot \frac{dF}{dt}\right) + B \cdot (J_2(\bar{\bar{\sigma}})) \cdot \frac{dF}{dt} \cdot e^{-Q_{ic}/R \cdot T} \ , \tag{5}$$

where

$d\varepsilon_{creep}/dt$ = total creep strain rate

$J_2(\bar{\bar{\sigma}})$ = second invariant of the deviatoric stress tensor

t = time

T = temperature

p = porosity

D_G = fuel grain size

$A_i, n_i, Q_i, B, \alpha, Q_{ic}$ = material parameters

i = subscript that is equal to 1 and 2 for each thermal creep stage

dF/dt = fission density rate

R = the universal gas constant.

The fission density rate leads to an induced creep effect [second term of Eq. (5)] with a low level of thermal activation energy (Q_{ic}), and an enhancement of the thermal creep (α). The material evolution due to irradiation is introduced into the model by the dependency of the material parameters on the burnup level and the porosity of the fuel pellet. Then, for the mechanical properties of the fuel pellet, the impact of porosity on the elastic and creep parameters is taken into account. In this respect, a poroviscoplastic compressible formulation for creep has been developed.[6]

Fuel cracking during irradiation and its coupling to viscoplastic behavior is taken into account through a nonunified formulation. Constitutive equations of the fuel-cracking model and its validation are detailed in Ref. 7. In order to represent fuel cracking in the pellet fragment, we have chosen a continuum approach. Once the yield stress is reached and until the complete rupture of the material elementary volume, the development of microcracking is represented by an instantaneous linear softening equation.

III.E.2. Cladding

The nonlinear behavior of the cladding under irradiation is taken into account by a nonunified formulation coupling a creep law [Eq. (6)],

$$\frac{d\varepsilon_v}{dt} = A \cdot (J_2(\bar{\bar{\sigma}}))^{n_p} \cdot e^{-Q_p/R \cdot T} \cdot e^{-B \cdot t} + C \cdot (J_2(\bar{\bar{\sigma}}))^{n_s} \cdot e^{-Q_s/R \cdot T} \cdot \Phi^p \ , \tag{6}$$

where

$d\varepsilon_v/dt$ = creep strain rate

Φ = fast neutron flux

$A, n_p, Q_p, B, C, n_s, p$ = material parameters

R = universal gas constant,

and a plasticity model similar to the example presented in Eq. (7),

$$J_2(\bar{\bar{\sigma}} - \bar{\bar{X}}) - R_0 \leq 0$$

and

$$\bar{\bar{X}} = \tfrac{2}{3} \cdot h \cdot \bar{\bar{\varepsilon}}_p \tag{7}$$

where

$\bar{\bar{X}}$ = internal stress associated with kinematics hardening

R_0 = yield stress

h = hardening modulus

$\bar{\bar{\varepsilon}}_p$ = plastic strain.

The creep rate enhancement due to the effect of the fast neutron flux Φ ($E > 1$ MeV) on the material is taken into account in the second term of Eq. (6), which models stationary creep. The irradiation-induced hardening of the material is introduced in the first term of Eq. (6), which models the primary creep, and by the dependency of the material parameters on neutron fluence. To account for the material behavior in the whole loading range, we use two different sets of material parameters for creep at a low stress level (base irradiation) and creep at a high stress level (ramp test). The anisotropic behavior of the cladding, which is particularly important for some alloys, can also be taken into account by using Hill's equivalent stress[8] instead of the Von Mises equivalent stress J_2 in Eqs. (6) and (7).

III.E.3. Pellet-Cladding Interface

Friction is of primary importance with respect to stress-or-strain concentration in the cladding[9,10] and regarding fuel cracking.[11,12] Measures of the friction coefficient between nonirradiated fuel materials and Zircaloy materials are usually within 0.4 to 0.7 and are almost independent of the contact pressure, temperature, and oxide thickness. Irradiation can enhance friction[11] and even lead to chemical bonding between the pellet and the cladding[12] at high burnup. In two-dimensional (2-D) and 3-D descriptions of the ALCYONE computation scheme, fuel pellet–cladding system unilateral contact is assessed by the Lagrangian multiplier method of the CAST3M finite element code, and a "Coulomb" model is introduced to take into account friction slip or adherence, according to the following equation:

$$v_t = \begin{cases} 0 & \text{if } \|F_t\| \le \mu \|F_n\| \\ -cF_t & \text{if } \|F_t\| = \mu \|F_n\| \end{cases} ,$$

where

v_t = slip rate

F_n = normal force

F_t = tangential force

μ = friction coefficient

c = positive number.

The dependence of the pellet-cladding friction coefficient to irradiation is also taken into account in the ALCYONE computation scheme.

IIIF. Chemical-Physical Behavior of Fuel Pellet

III.F.1. Solid Swelling and Densification

Volume variation due to solid swelling and densification is computed with Eq. (8), where the strain rate is computed with the unit tensor and a function of the pellet burnup:

$$\dot{\bar{\bar{\varepsilon}}}_{SS\_D} = f(BU, \ldots) \cdot \bar{\bar{I}} \ . \tag{8}$$

Solid swelling is linked to solid fission products that tend to modify the crystallographic dimensions of uranium dioxide.[2] The densification process is the result of the annihilation of small pores caused by the activation energy of fission peaks.[13]

III.F.2. Behavior of Gaseous Fission Products

The behavior of gaseous fission products is modeled by different approaches:

1. a semiempirical model for the simulation of integral tests[14]
2. advanced models for detailed interpretation of laboratory results.[15]

The constitutive equations presented in this paper are simplified in order to illustrate the main phenomena taken into account in the simulation of gaseous fission product behavior. A complete description of the constitutive equations used in the MARGARET advanced model of the PLEIADES platform can be found in Ref. 15.

III.F.2.a. Steady-State Irradiation Conditions. Under steady-state loading conditions at low burnup, gaseous swelling is derived from the empirical expression given by Eq. (9):

$$tr[\dot{\bar{\bar{\varepsilon}}}_{GS}^{ST}] = f(T) \cdot (1 - e^{k \cdot \rho \cdot BU}) \ , \tag{9}$$

where

k = adjustable parameter

ρ = density (kg U/m^3)

BU = burnup (MWd/kg U).

Because of the low stress level in the pellet under nominal irradiation, there is no coupling effect with the mechanical state needed in Eq. (9). At the same time, other constitutive equations, not detailed here, are used to compute the quantity of fission gas produced and its location (intragranular, intergranular, or released).

III.F.2.b. Transient State Irradiation Conditions. Gaseous swelling under transient state irradiation conditions is derived from a nonlinear time differential system composed of Eqs. (10), (11), and (12):

Balance equation for fission gas product transfer:

$$f_i(C_{res}, \dot{C}_{res}, C_{b_j}, \dot{C}_{b_j}, G_{b_j}, \dot{G}_{b_j}, C_{ird_k}, \dot{C}_{ird_k}) = 0 \ ; \quad (10)$$

Gas state equations:

$$gfpse\left(\sigma^{b_j}_{interface}, r_{b_j}, \frac{G_{b_j}}{C_{b_j}}, T\right) = 0 \ ; \quad (11)$$

Constitutive equations for pressurized cavity behavior in solid medium:

$$gs\left(\sigma^{b_j}_{interface}, \bar{\bar{\sigma}}_M, \frac{dr_{b_j}}{dt}, T, \ldots\right) = 0 \ , \quad (12)$$

where

C_{res} = gas concentration per unit volume of fuel (mol/m^3) located in UO_2 atomic network

C_{b_j} = bubble concentration per unit volume of fuel; subscript j describes the bubble type and size

G_{b_j} = gas concentration per unit volume of fuel (mol/m^3) located in bubble of type and size j

C_{ird_k} = default (void, interstitial, dislocation) concentration per unit volume of fuel; subscript k describes the default type

$\sigma^{b_j}_{interface}$ = normal stress at the gas-solid interface for bubble type and size j

r_{b_j} = radius of bubble type and size j

T = local gas temperature

$\bar{\bar{\sigma}}_M$ = effective Cauchy stress tensor in the bulk material.

The unknown functions of the differential equation system (10) are internal state variables describing material changes and gaseous fission product transfer under irradiation. The fission product gas state equation (11) and the pressurized cavity behavior constitutive equation (12) assess the bubble mechanical state.

IIIG. Coupling of Gaseous Swelling and Mechanical Behavior

III.G.1. Approach

The coupling problem between mechanical behavior and gaseous fission product behavior at time t can be decomposed as follows:

Mechanical equilibrium equations:

$$\begin{cases} \text{div } \bar{\bar{\sigma}}_M = 0 \text{ on } \Omega \\ \bar{\bar{\sigma}}_M \cdot \vec{n} = \vec{\phi}_{BC} \text{ on } \partial\Omega_\phi \\ \vec{u} = \vec{u}_{BC} \text{ on } \partial\Omega_u \end{cases} ; \quad (13)$$

Mechanical nonlinear behavior:

$$\frac{d\bar{\bar{\sigma}}_M}{dt} = \underline{\underline{E}} : \left(\frac{d\bar{\bar{\varepsilon}}_t}{dt} - \frac{d\bar{\bar{\varepsilon}}_{crack}}{dt} - \frac{d\bar{\bar{\varepsilon}}_{creep}}{dt} - \frac{d\bar{\bar{\varepsilon}}_{GS}}{dt}\right) \ ; \quad (14)$$

Gaseous fission product behavior:

$$\frac{d\bar{\bar{\varepsilon}}_{GS}}{dt} = f_{GS}(\bar{\bar{\sigma}}_M) \ , \quad (15)$$

where

Ω = domain used to describe the fuel element geometry

$\partial\Omega_\phi$ = frontier with force boundary conditions $\vec{\phi}_{BC}$

$\vec{n}$ = normal vector to $\partial\Omega_\phi$

$\partial\Omega_u$ = frontier with displacement boundary condition $\vec{u}_{BC}$

$\bar{\bar{\varepsilon}}_t$ = total strain

$\bar{\bar{\varepsilon}}_{crack}$ = crack strain

$\bar{\bar{\varepsilon}}_{creep}$ = creep strain

$\bar{\bar{\varepsilon}}_{GS}$ = gaseous swelling strain

$f_{GS}(\bar{\bar{\sigma}})$ = differential equation system for gaseous fission product behavior, Eqs. (10), (11), and (12).

From a practical point of view, the time integration of the multiphysics problem is derived from an incremental formulation, between times t and $t + \Delta t$, along the irradiation loading time history.

Because the constitutive gaseous swelling equations $f_{GS}(\bar{\bar{\sigma}})$ cannot be easily introduced into Eq. (14), an external iteration process has to be achieved between the mechanical problem, Eqs. (13) and (14), and the gaseous swelling problem, Eq. (15). This iteration process is based on the fixed-point method where the coupling variables are the effective stress in the bulk material and the gaseous swelling strain variation during time step Δt. In this approach we assume that the gaseous swelling strain rate in Eq. (14) is constant and can be computed as

$$\frac{d\bar{\bar{\varepsilon}}_{GS}}{dt} = \frac{\int_t^{t+\Delta t} f_{GS}(\bar{\bar{\sigma}}) \cdot dt}{\Delta t} \ .$$

IV. NUMERICAL SIMULATION OF PWR FUEL ROD BEHAVIOR UNDER IRRADIATION

IVA. Pellet-Cladding Gap Closure Mechanisms and Fuel Element Behavior Under Irradiation

The mechanisms leading to pellet-cladding gap closure and ridge formation in the cladding during base irradiations and power ramp tests can be schematically decomposed as described in Secs. IV.A.1 and IV.A.2 (Ref. 16).

IV.A.1. Base Irradiation

During the first power increase, the thermal gradient associated with the fuel fragmentation is at the origin of the hourglass shape of the pellet. The consequence is a reduction of the gap at the interpellet plane (see Fig. 3a). Then, during the power hold period, the fuel element dimensions will change because of the following phenomena:

1. densification and solid swelling in the pellet
2. cladding creep under a compressive stress state.

The competition between these geometrical changes leads to a gap decrease with mainly two steps of PCI:

1. low interaction stage with a gap partially closed in the vicinity of the interpellet plane
2. strong interaction stage with a gap entirely closed and a significant contact pressure level (see Fig. 3b).

During the interaction period the pellet hourglass shape is printed in the cladding because of its inelastic strains due to material creep under external pressure loading. Moreover, the cladding diameter decrease can also tend to reduce the extent of pellet hourglass magnitude, thanks to stress relaxation due to irradiation-induced creep in the pellet fragment. Through this analysis, it appears that the magnitude of cladding primary ridges at the end of base irradiation is the result of the competition between cladding and pellet creep. The development of a high-burnup structure in the pellets with pronounced gas swelling can smooth the radial deformation of the cladding after base irradiation (see Ref. 17).

IV.A.2. Power Ramp Test

The behavior of fuel rods during ramp testing depends on many factors: the geometry of the fuel pellet (height/diameter ratio of the pellet, dish volume, chamfer dimensions, etc.), the power history (maximum power, increase of power, power rate, duration of holding period, etc.), the thermomechanical behavior of fuel and cladding (burnup of the pellet, thermal expansion of the fuel pellet, cladding creep and plasticity, fuel creep, etc.), and fission gas swelling in the fuel pellet.

The diameter increase of the cladding during power ramp is driven by the thermal expansion of the pellet and by fission gas swelling if the temperature of the pellet is high enough. The contribution of gas swelling can be important particularly if the holding period is long (>20 to 30 min) or if the fuel rod has a high burnup. Cladding expansion during ramp testing is first induced at the interpellet level because of the hourglass of the pellet resulting from the thermal gradient (see Fig. 4a), but soon, it is compensated by dish filling because of creep and fission gas swelling of UO_2. If the height/diameter ratio of the pellet is large (>1.5), the impact of dish filling creep on the midpellet plane will be small. Radial expansion will therefore be maximum at the midpellet level since dish filling will limit radial expansion at the interpellet level (see Fig. 4b). This is the reason why the midpellet ridges observed in the database can reach significant values (30 μm) and often exceed their interpellet counterparts by a factor 2 or 3; see Fig. 5. This is not the case with pellets of smaller height/diameter ratio (~1) as was shown with ALCYONE 3D in Ref. 17 since dish filling has in this case consequences on the deformation of the midpellet plane due to axial creep. Hourglass-induced strains therefore remain predominant in this configuration leading mainly to interpellet ridges.

The kinetics of midpellet ridge development strongly depend on the maximum power and temperature reached during ramp testing since radial expansion of the pellet and dish filling depend on these two parameters. Figure 6 gives the midpellet diameter increase of the pellet during the transient part of the ramp test due to the total swelling of the fuel pellet as a function of the maximum temperature of the pellet. Also plotted in Fig. 6 is the calculated dish filling as a function of the maximum temperature. As can be seen in Fig. 6, when the pellet maximum temperature is >1900°C, the diameter tends to an asymptotic value. A threshold temperature can also be defined for complete filling up of the dishing (>70%) in the 3-D simulations. It is close to 1700°C and hence of the same order as the temperature threshold for fission gas swelling activation. Simulation results indicate furthermore that 100% dish filling is usually reached within a few minutes during the holding period if the power is sufficiently high.

This kind of interpretation (cladding ridges, dish filling, etc.) would not be possible without a 3-D model of the pellet fragment. Moreover, the 3-D simulation enabled us to develop a simplified pellet hourglassing model,[18] with partial reversibility in case of power drop, for the generalized plane strain approach of the 1-D axisymmetric representation or the 2-D r-θ representation. Thanks to this simplified model, the pellet temperature can be assessed with reasonable accuracy in these simplified representations.

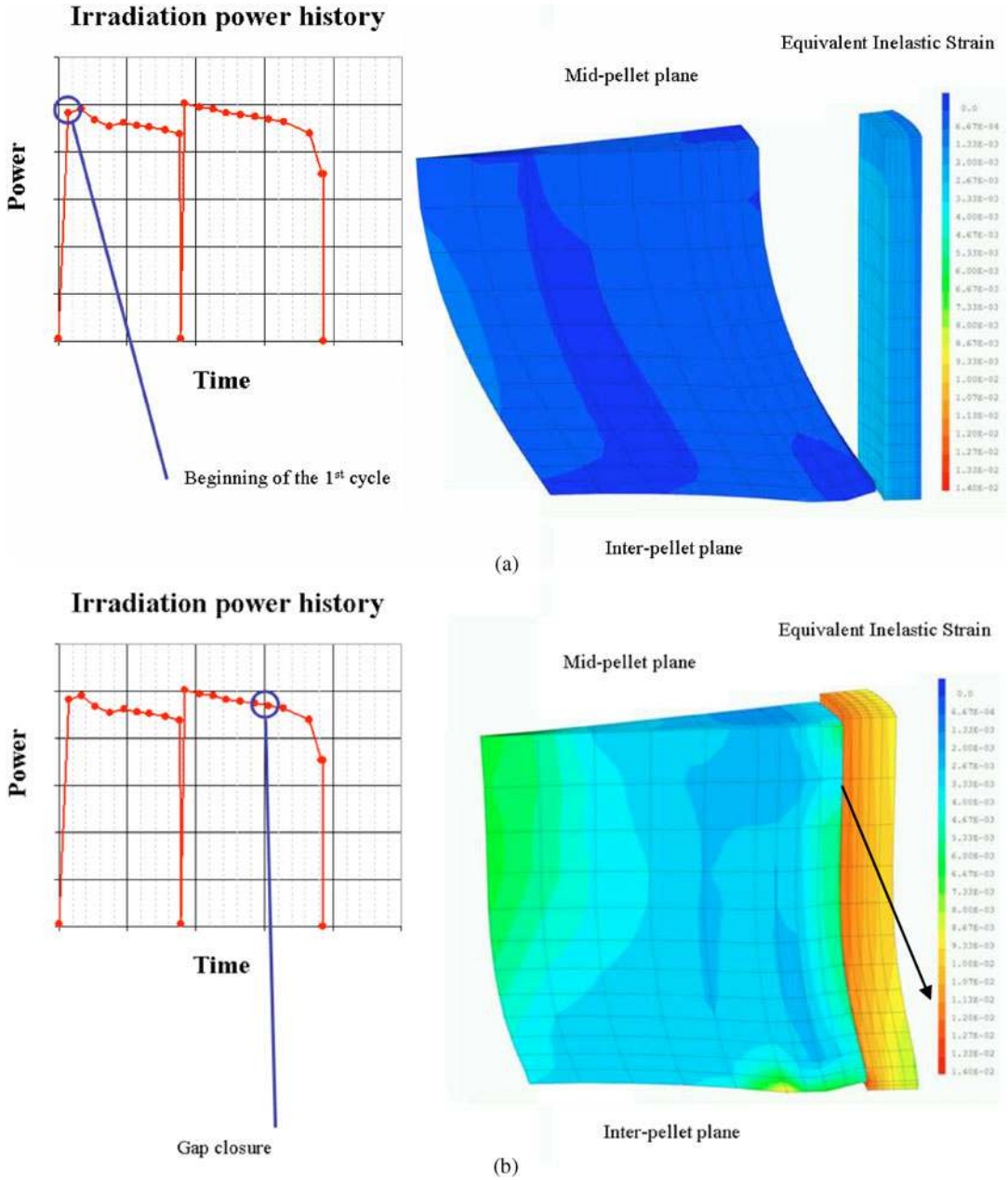

Fig. 3. Pellet-cladding gap closure and cladding ridging mechanisms under base irradiation: (a) hourglass shape at the end of the first power increase and (b) complete gap closure during the second cycle.

IVB. Validation of the Simulation with Residual Displacement Measurement

Postirradiation examinations (PIEs) include measurements of the residual diameters and height of interpellet and midpellet ridges after base irradiation and power ramp tests, estimations by optical microscopy of dish filling of the pellet, and estimations of the number of radial cracks after ramp tests. The data from cladding outer profilometry are interesting because they give quantitative elements on the pellet-cladding mechanical interaction that can lead to a significant number of residual strains in the cladding. A comparison between computation and experimental measurements of the cladding outer diameter before and after the power ramp test is presented in Fig. 7. As shown in Ref. 19, the 3-D simulation has a good capacity to assess the external cladding profilometry variation after base and ramp test irradiations (residual diameters, height of interpellet and midpellet ridges).

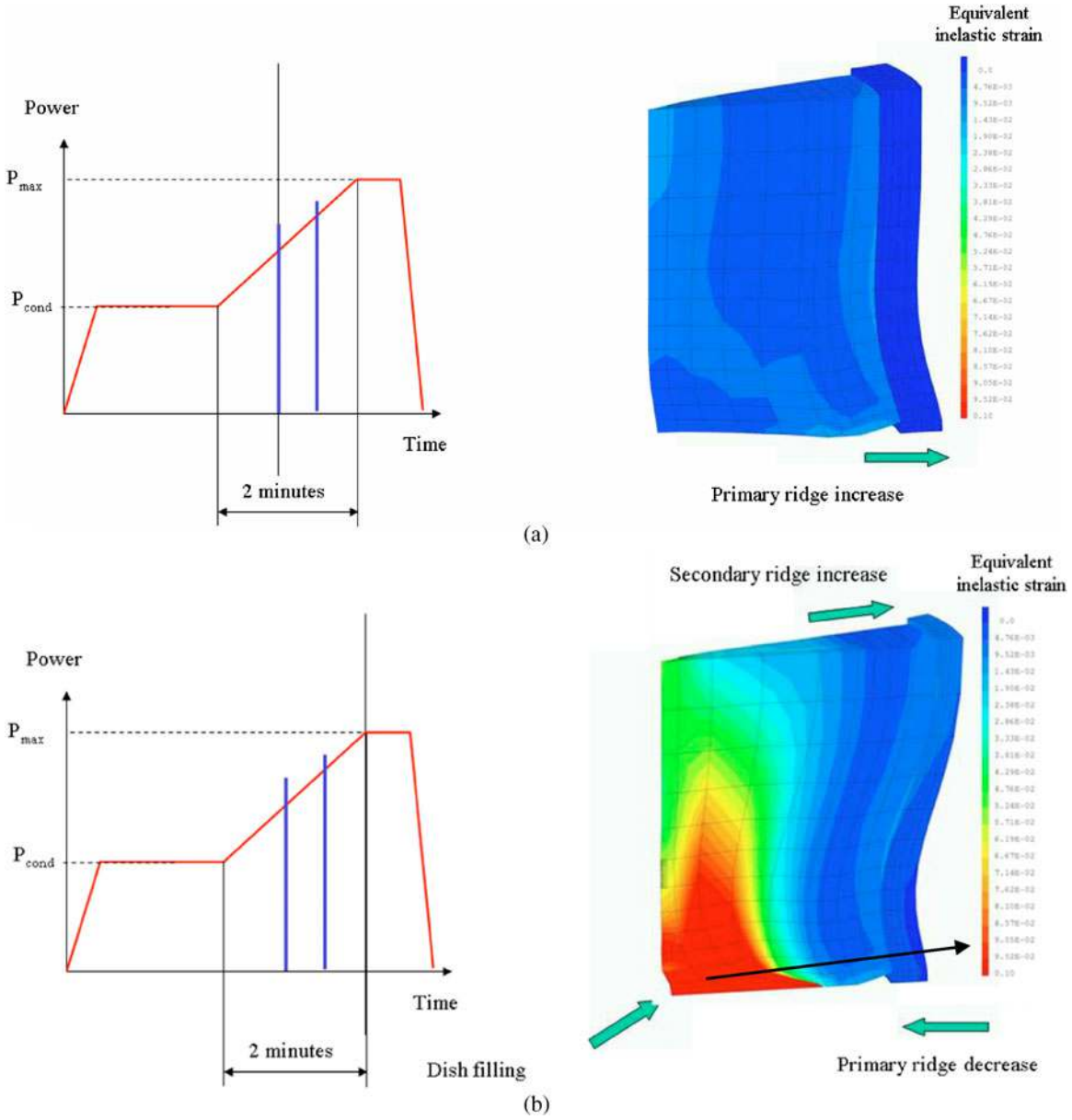

Fig. 4. Pellet viscoplasticity and cladding ridging mechanisms under power ramp test: (a) primary ridge increase at the beginning of the power transient and (b) impact of viscoplasticity at the end of the power transient.

The behavior of the fuel pellet at the interpellet level is rather complex since it results from a compromise between the pellet thermal and gas-induced swelling, which tends to increase the diameter, and the filling up of the dishing due to UO_2 creep at high temperature, which tends to reduce the diameter expansion. Therefore, data concerning dish filling are important to check that creep rates of the fuel element are correctly estimated (overestimated dish filling would lead to underestimated interpellet ridges and interpellet diameters).

Figure 8 gives an overview of the 3-D calculated dish fillings (residual) after ramp testing compared to experimental estimations. The experimental estimates are separated into four categories: dish filling $<10\%$, dish filling between 20% and 30%, almost complete dish filling ($>90\%$, small residual opening), and 100% dish filling. The classification of the fuel rods in one or the other category depends on the power history and on the duration of the holding period during ramp tests. Figure 8 shows that the calculated dish fillings are qualitatively well estimated since their evolution is similar to that of experimental measures. In particular, small dish fillings ($<30\%$) obtained on ramp tests with no holding periods are very well estimated.

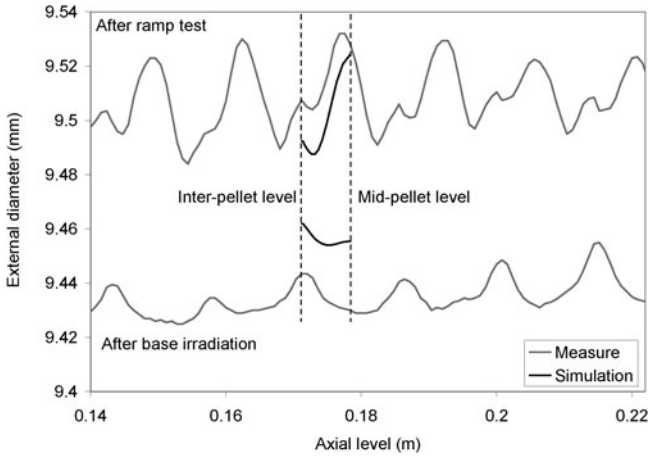

Fig. 5. The 3-D calculated and measured ridges after base irradiation and ramp testing showing the important development of the midpellet ridge during ramp testing.

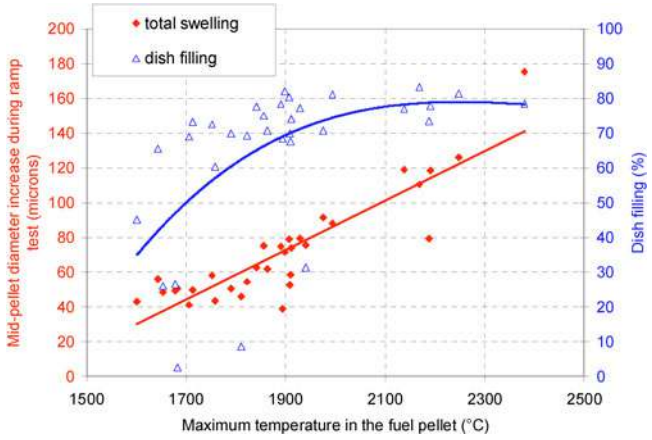

Fig. 6. Pellet diameter increase and dish filling during a power ramp test.

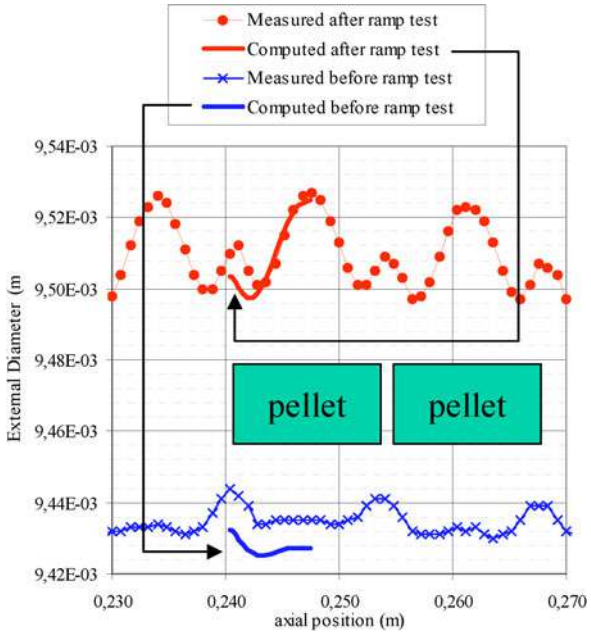

Fig. 7. Experimental and computed axial variations of the cladding outer diameter after irradiation.

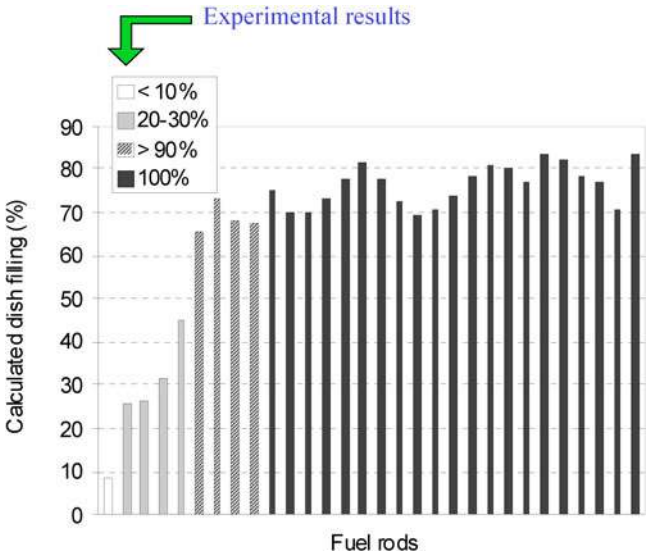

Fig. 8. Calculated and estimated dish filling at the end of ramp tests.

IVC. Pellet Cracking Under Irradiation

Fuel pellet fragmentation occurring at an early stage of irradiation and due to thermal stresses is taken into account through a 3-D finite element model and its boundary conditions in the ALCYONE computation scheme. For secondary cracks occurring inside the pellet fragment, a continuum damage model is used according to the constitutive equations given in Ref. 7. Simulation results for secondary crack pattern assessment during a power ramp test are summarized in Fig. 9. The latter shows that an axial crack (perpendicular to the axial direction) located at the midpellet plane appears at the end of base irradiation. This crack is initiated in the simulation because of a tensile residual axial stress at the fragment center after shutdown. In the power ramp test, at the beginning of the holding period at the maximum power level, this axial crack is closed, because of the thermal gradient that leads to compressive stresses around the fragment central axis. New axial and circumferential cracks have been initiated on the fragment outer part submitted to biaxial tensile stresses. After the ramp test, axial cracks initiated at the maximum power level in the outer part of the fragment are closed, and the axial crack

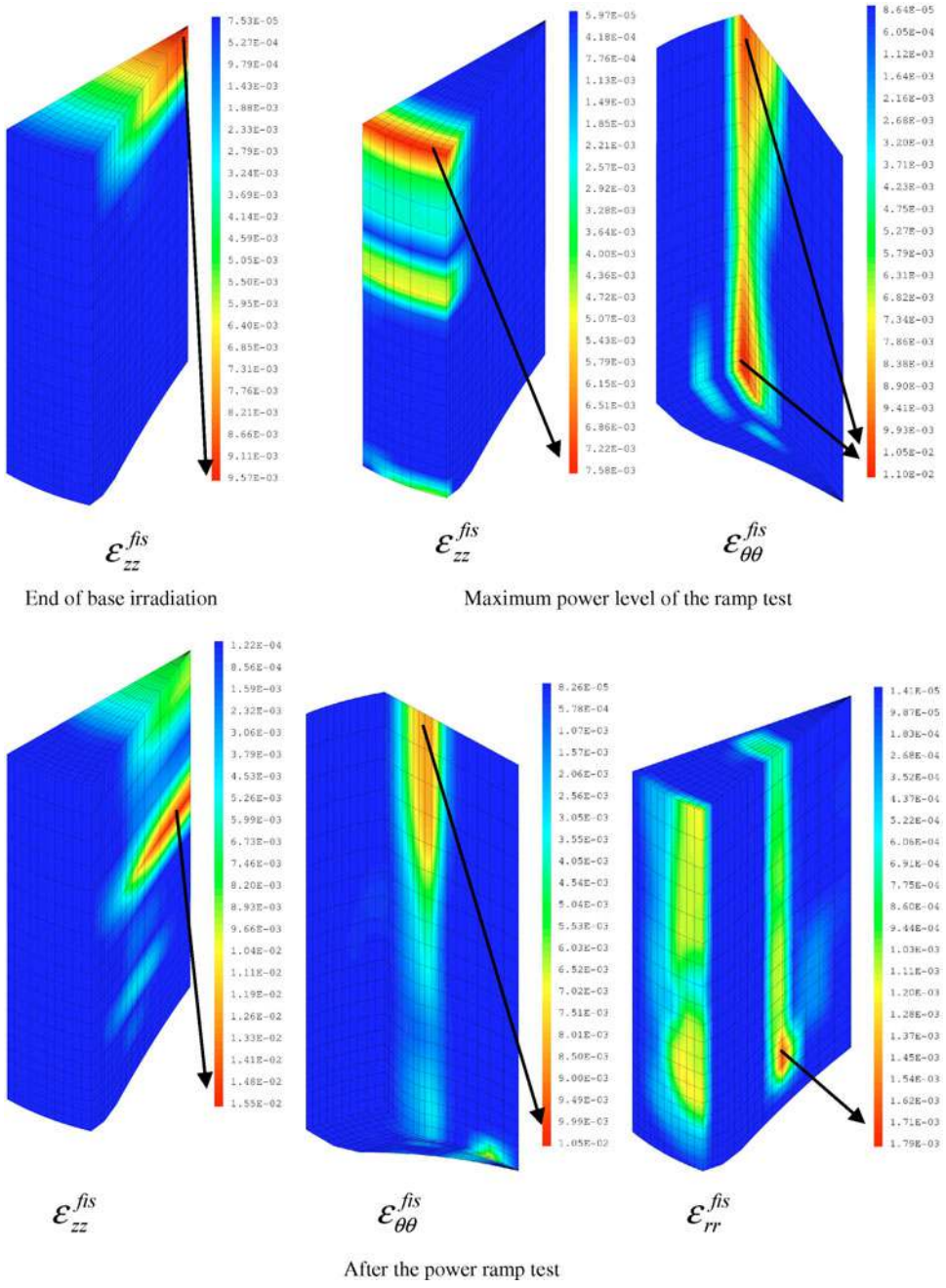

Fig. 9. Secondary crack pattern assessment during a power ramp test.

initiated at the end of base irradiation is reopened in the fragment center with new axial cracks initiated during reverse loading at the end of the power ramp test. Residual opening of the circumferential cracks initiated at the maximum power level is reduced after shutdown of the power ramp test, and radial cracks (perpendicular to the radial direction) are initiated on the outer part and at an intermediate radius. The latter is approximately the same as the radius reached by the circumferential cracks initiated from the pellet outer part.

IVD. Benchmark with Other Fuel Performance Codes

Benchmarking for the PLEIADES platform's applications comes either from the results of studies achieved with the CEA's first-generation fuel performance code METEOR, which has been fully implemented in the 1-D option of ALCYONE application, or from the results of recent studies achieved with ALCYONE. For METEOR and ALCYONE some results have been presented in the framework of the Studsvik Cladding

Integrity Program (SCIP) project[17] with power ramp tests performed on high-burnup recrystallized Zircaloy2–UO_2 boiling water reactor fuel rods. In this paper, simulation results of METEOR are in good agreement with experimental results for profilometry and fission gas releases. Moreover, for the SCIP benchmark ALCYONE was the only available 3-D fuel performance code, and the ridge assessments after base irradiation and power ramp testing were consistent with experimental results. Still, for the SCIP project, the ALCYONE results have been compared with other fuel performance codes, such as FALCON-PSI, FRAPCON-3 v3.3, and STAV7.3, in Ref. 20. In the latter, ALCYONE results concerning diameter increase during ramp tests are comparable to other fuel performance codes despite the benchmark study not being representative of ALCYONE's validation domain, which is more focused on PWR fuel rods. For cladding elongation it is noticed that ALCYONE behavior is not as far qualitatively and quantitatively as the other codes. This good behavior is attributed in Ref. 20 to the sophisticated models for pellet creep and cracking included in ALCYONE.

Recently, ALCYONE simulation results have been presented in Ref. 21 for reactivity-initiated-accident experiments performed in the CABRI facility in the framework of a first international program called "CABRI REP Na." This paper shows that the results of the 1-D computation scheme of ALCYONE are in good agreement with experimental measurements for the cladding axial profilometry, sodium temperature variations, and fuel rod elongation during the pulse testing. Results of the 3-D computation scheme of ALCYONE are also presented and are able to reproduce the experimental measurement for the ridge height and the dish filling.

V. LOCAL STRESS-AND-STRAIN COMPUTATION FOR PCI MODELING

Thanks to the 3-D finite element model, the local mechanical state involved during PCI at the cladding inner wall can be computed. As shown in Fig. 10, the critical zone for SCC initiation is located at the interpellet plane in front of a fuel crack between two pellet fragments. Because of the pellet hourglass shape, the contact pressure and the shear stress at the pellet-cladding interface are maximum in this critical zone. The stress-and-strain concentration derived from the 3-D computation is consistent with this experimental observation. However, an accurate computation of the local mechanical stress concentration cannot be achieved using the standard mesh refinement technique. The latter leads to a prohibitive computation time for meshes required for a given accuracy. The mesh refinement aspect is discussed in Ref. 22 through the PCI rupture criterion and is illustrated in the Fig. 11 with an assessment of crack opening between two pellet fragments. This result shows that in order to have at least ten elements to describe the contact singularity, the mesh size required in the critical zone is ~ 1 μm. A

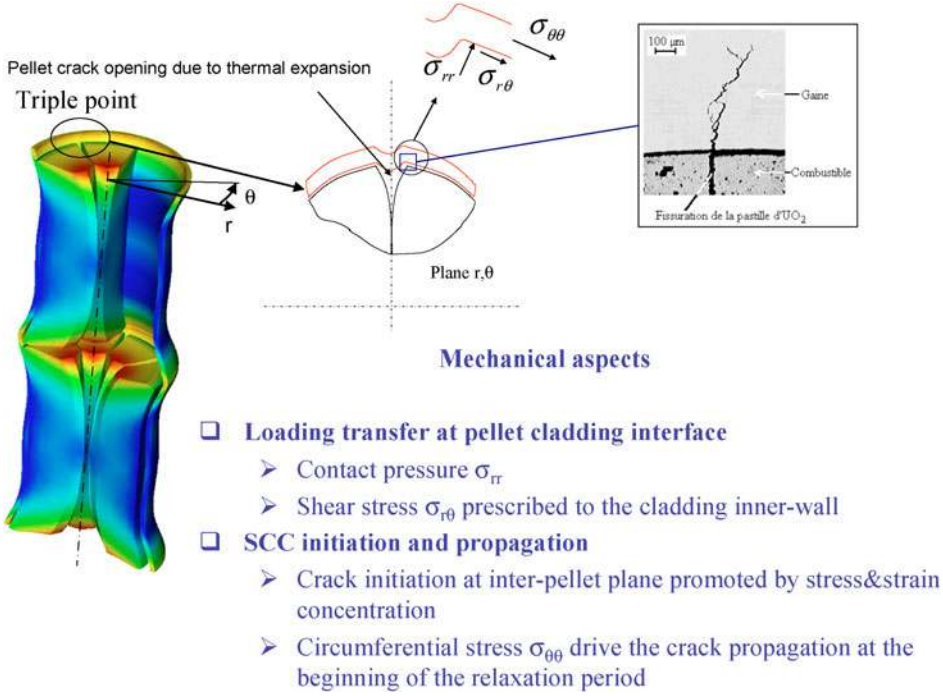

Fig. 10. Local approach for SCC simulation under PCI loading.

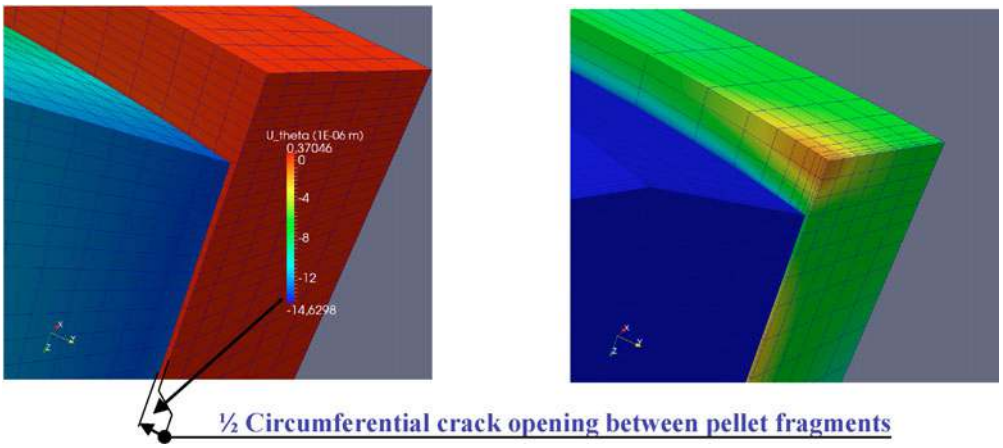

Fig. 11. Mesh refinement needed for an accurate description of the contact singularity.

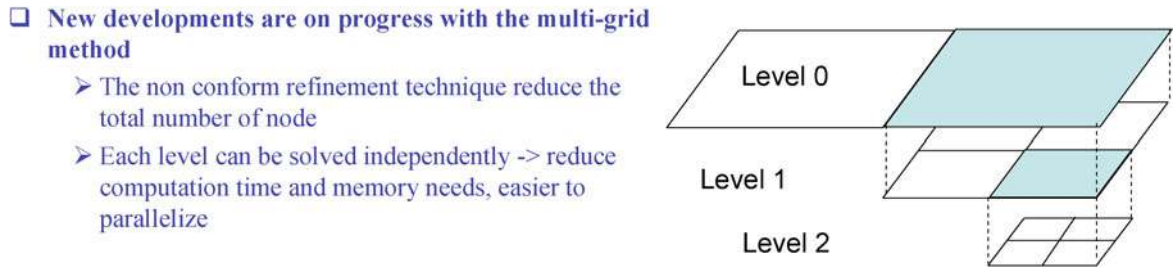

Fig. 12. Multigrid method under development in the PLEIADES platform.

new mesh refinement technique called the multigrid method, under development in the PLEIADES platform, will overcome this limitation. The multigrid method (see illustration in Fig. 12) can use a nonconform mesh refinement that reduces the total number of nodes, compared to a standard mesh, for a given accuracy. The multilevel algorithm of the multigrid method also offers an interesting potential for parallelization in order to reduce computation time and to optimize memory needs.

VI.CONCLUSIONS

The PLEIADES fuel performance software environment has been under development for 10 yr; eight computation schemes are now under operation. Concerning PCI simulation, physical models can be validated and improved thanks to the multidimensional computation scheme ALCYONE of the PLEIADES platform. ALCYONE provides a detailed analysis of fuel element behavior and enables validation through comparing simulation and PIE results (cladding residual diameter and ridges, dish filling, pellet cracking, etc.). In the last few years the 3-D computation scheme of the ALCYONE application has been enriched with a complete set of physical models to take into account the thermomechanical and the chemical-physical behavior of the fuel element under irradiation. These models have been validated through the ALCYONE application on a large experimental database composed of approximately 400 study cases. The strong point of the ALCYONE application concerns the stress-and-strain concentration involved in the local approach of SCC rupture under PCI, which can be computed with the 3-D finite element solver CAST3M embedded in the PLEIADES platform.

Further developments for PCI modeling in the PLEIADES platform are devoted to a new mesh refinement method (multigrid method[23]) and a new component for assessing fission product chemical recombination.

REFERENCES

1. D. PLANCQ et al., "PLEIADES: A Unified Environment for Multi-Dimensional Fuel Performance Modelling," *Proc. Int. Mtg. Light Water Reactor Fuel Performance*, Orlando, Florida, September 19–22, 2004, American Nuclear Society (2004).

2. C. STRUZIK, M. MOYNE, and J.-P. PIRON, "High Burnup Modelling of UO2 and MOX Fuel with METEOR/TRANSURANUS Version 1.5," *Proc. Int. Mtg. Light Water Reactor Fuel Performance*, Portland, Oregon, March 2–6, 1997, p. 126, American Nuclear Society (1997).

3. I. M. PALMER, K. W. HESKETH, and P. A. JACKSON, "A Model for Predicting the Radial Power Profile in a Fuel Pin," *Proc. Specialists' Mtg. Water Reactor Fuel Element Performance Computer Modelling*, Preston, United Kingdom, International Atomic Energy Agency (1992).

4. P. REUSS, "Base de neutronique—Migration des neutrons," BN 3014, Technique de l'Ingénieur (2005).

5. F. LEMOINE, D. BERNARD, and E. FEDERICI, "Validation Assessment of Neutron Calculations for Radial and Azimuthal Distributions of Actinides and Fission Products in PWR Rods," presented at 2011 Water Reactor Fuel Performance Mtg., Chengdu, China, September 11–14, 2011.

6. Y. MONERIE and J. M. GATT, "Overall Viscoplastic Behaviour Of Non Irradiated Porous Nuclear Ceramics," *Mech. Mater.*, **38**, 608 (2006).

7. B. MICHEL et al., "3D Fuel Cracking Modelling in Pellet Cladding Mechanical Interaction," *Eng. Fracture Mech.*, **75**, 3581 (2008).

8. A. SONIAK et al., "Irradiation Creep Behavior of Zr-Base Alloys," *Zirconium in the Nuclear Industry: 13th International Symposium*, ASTM STP 1423, p. 837, G. D. MOAN and P. RUDLING, Eds., ASTM International, West Conshohocken, Pennsylvania (2002).

9. G. ROBERTS, "The Concentration of Stress in Cladding Produced by the Expansion of Cracked Fuel Pellets," *Nucl. Eng. Des.*, **47**, 257 (1978).

10. J. BROCHARD et al., "Modelling of Pellet Cladding Interaction in PWR Fuel," *Trans. SMIRT 16* (2001).

11. E. SMITH, "The Fuel-Cladding Interfacial Friction Coefficient in Water-Cooled Reactor Fuel Rods," *Trans. SMIRT 5* (1979).

12. J. C. WOOD, B. A. SURETTE and I. AITCHISON, "Pellet Cladding Interaction—Evaluation of Lubrification by Graphite," *J. Nucl. Mater.*, **88**, 81 (1980).

13. A. BOULORE, "étude et modélisation de la densification en pile des oxydes nucléaires UO2 et MOX," Thesis, Ecole Nationale Supérieure des Mines de Saint-Étienne, Institut National Polytechnique de Grenoble (2001).

14. Ph. GARCIA, C. STRUZIK, and M. AGARD, "The Effect of Fission Gas Swelling on Cladding Strains During Power Ramp Tests," *Proc. Conf. Fuel Chemistry and Pellet Cladding Interaction Related to High Burn-Up Fuel*, Nyköping, Sweden, September 7–10, 1998, IAEA TECDOC 1179, International Atomic Energy Agency (1998).

15. L. NOIROT, "MARGARET: An Advanced Mechanistic Model of Fission Gas Behaviour in Nuclear Fuel," *Nucl. Eng. Des.*, **241**, *6*, 2099 (2011).

16. B. MICHEL, "PCMI Assessment Using 3D Modelling," *Trans. SMIRT 18* (2005).

17. J. SERCOMBE, et al., "1D and 3D Analyses of the Zy2 SCIP BWR Ramp Tests with the Fuel Codes METEOR and ALCYONE," *Nucl. Eng. Technol.*, **41**, *2* (Mar. 2009).

18. P. GARCIA et al., "Mono-Dimensional Mechanical Modelling of Fuel Rods Under Normal and Off-Normal Operating Conditions," *Nucl. Eng. Des.*, **216**, *1–3*, 183 (July 2002).

19. J. SERCOMBE et al., "Multi-Dimensional Modeling of PCMI During Base Irradiation and Ramp Testing with ALCYONE V1.1," *Proc. Top Fuel 2009*, Paris, France, September 2009.

20. L. E. HERRANZ et al., "Assessment of Fuel Rod Performance Codes Under Ramp Scenarios Investigated Within the SCIP Project," *Nucl. Eng. Des.*, **241**, *3*, 815 (Mar. 2011).

21. J. SERCOMBE et al., "1D and 3D Modeling of PCMI During a RIA with ALCYONE V1.1," *Proc. Top Fuel 2010*, Orlando, Florida, September 2010.

22. B. MICHEL, J. SERCOMBE, and G. THOUVENIN, "A New Phenomenological Criterion for Pellet Cladding Interaction Rupture," *Nucl. Eng. Des.*, **238**, 1612 (2008).

23. L. BARBIE et al., "AMR Methods in Solids Mechanics for Pellet-Cladding Interaction Modeling," presented at European Community in Computational Methods in Applied Sciences Int. Conf. Adaptive Modeling and Simulation (ADMOS 2011), Paris, France, June 6–8, 2011.